Mechanical Testing

Tanju Teker*, S. Osman Yılmaz and Ercan Bulus

Effect of alloying elements on mechanical behaviour of Cu-Zn-Sn bronzes

https://doi.org/10.1515/mt-2022-0433

Abstract: The effect of Fe, P and Mn on microstructure and fatigue properties of CuZnSn bronzes investigated with optical microscopy and scanning electron microscopy, energy dispersive spectroscopy, X-ray diffraction, hardness, tensile and fatigue tests. The addition of Fe, Mn and P to Cu-Zn-Sn bronzes formed $Cu_{31}Sn_8$, Cu_6Sn_5, $ZnSn_2$, $PbSnS_2$, ZnS, Cu_2S, $FeZn_9$ and $FeZn_{21}$ phases. These phases were deposited between the dendrite arms and were dissolved in the matrix in small amounts. Especially, these precipitated phases were effective in fatigue properties. The formation of Cu-Sn, Cu-Zn and Zn-Sn intermetallic phases emitted due to the addition of Fe, Mn and P increased the fatigue strength. The spread of ferrous phases caused an increase in mechanical properties. The beneficial effect of P addition on the fatigue life far surpassed that of Mn and Fe additives.

Keywords: fatigue life; hardness; microstructure; Sn-Cu bronzes; tensile strength.

1 Introduction

Sn-Cu bronze's self-lubricating, high strength, wear and corrosion resistance properties made it preferred in various tribological areas. Sn-Cu bronze is used in the chemical industry, shafts, machine production, gears and crankshaft bearings. Additives such as Sn and Cu are used in a ratio of 4–6 wt% and 2–3 wt% ranges, respectively [1–3]. In addition, the reason for adding Zn is to increase fluidity during casting. However, it is preferable to use Cu addition in applications where fatigue is affected by corrosion. Cyclic loads affect the wear surface more than static loads. Generally, fatigue cracks the nuclei where stress levels are high. The process in these places creates fatigue lines that characterize the behaviour of crack formation depending on the loading conditions and environment [4–7]. In addition, the parameters increasing tensile strength also increases fatigue life. Abrasion resistant alloys contain intermetallic phases reinforced with soft matrix. Therefore, good results can be obtained from the energy absorption properties of the soft phase and the corrosion resistance of the hard metal phases. The hard particles in these alloys carry the shear energy to the soft matrix. On the contrary, the energy consumed for wear is reduced. As a result, these materials exhibit high wear resistance. On the other hand, these structures are not preferred for applications subject to conditions with cyclical loads [8–12]. Hebesberger et al. [13] reported that they deformed pure copper by high pressure torsion. As the stress increased, the size of the elements decreased and the steady state value was reached. The steady state size decreased with increasing pressure and decreasing temperature. Misdirection between neighbouring structural elements increased with tension and eventually reached an almost random distribution.

The aim of this study was to create a structure with hard phases in the soft matrix by adding Fe, Mn, P elements as intermetallic phase formers with different content. Afterward, effect of alloying elements on the fatigue life and microstructure of Cu-Zn-Sn bronzes was examined.

2 Experimental

High purity Cu, Sn and Zn (99.99%) powders were chosen for this study. The elemental powders for the alloy were melted in a high-frequency induction furnace under argon atmosphere. The melts were then poured into a cylindrical mold 10 mm in diameter. Their chemical compositions are shown in Table 1. The intersection surfaces of the samples for metallographic examinations were etched with nital. Microstructures of the samples were examined by optical microscopy (OM: LEICA DM750), scanning electron microscopy (SEM: ZEISS EVO LS10). Element contents of the

***Corresponding author: Tanju Teker**, Department of Manufacturing Engineering, Faculty of Technology, Sivas Cumhuriyet University, 58140, Sivas, Türkiye, E-mail: tanjuteker@cumhuriyet.edu.tr
S. Osman Yılmaz, Department of Mechanical Engineering, Faculty of Engineering, Tekirdag Namık Kemal University, 59160, Corlu, Tekirdag, Türkiye
Ercan Bulus, Department of Computer Engineering, Faculty of Engineering, Tekirdag Namık Kemal University, 59160, Corlu, Tekirdag, Türkiye

Table 1: Chemical compositions of samples.

Sample no	Element (wt%)							
	Cu	Sn	Zn	Pb	Fe	Mn	P	S
S1	Bal.	5.60	6.30	0.40	–	–	–	0.020
S2	Bal.	5.75	5.85	0.45	0.015	–	0.074	0.032
S3	Bal.	5.56	5.46	0.46	1.045	–	0.080	0.016
S4	Bal.	5.43	5.38	0.01	–	0.243	–	0.012
S5	Bal.	5.33	6.27	0.40	–	–	0.078	0.045
S6	Bal.	5.27	6.93	0.45	–	–	0.176	0.032
S7	Bal.	5.46	4.75	0.46	–	–	0.182	0.031

samples were determined by energy dispersive spectroscopy (EDS). The phases and compounds formed in the samples were determined by X-ray diffraction (XRD: Bruker). Tensile samples were made according to ASTM E8-78 L_0 = 4D and testing was done on a Shimadzu testing machine at a speed of 0.5 mm min^{-1}. In addition, yield, tensile strength, elongation and toughness values were determined by performing the tensile test. Low cycle fatigue tests were performed using an MTS hydraulic testing machine operating at a voltage ratio of 0.1 and a frequency of 10 Hz. Microhardness rates were detected using a 50 g load at 0.5 mm intervals on the Brinell scale on the QNESS Q10M hardness device.

3 Results and discussion

3.1 Effect of Fe on microstructure

Optical and scanning electron micrographs of the microstructures of S1 and S2 samples are given in Figure 1a–c. The main matrix of these samples was α-Cu. As seen in Figure 1, large blocks of Cu-Sn and Cu-Zn phases were formed between the arrows of the dendrites and (Zn, Cu) S (black) phases were detected in these phases. In addition, EDS analysis of these samples (Figure 2) represented the presence of Zn, Sn and S elements in the matrix.

The SEM micrographs of S3 are given in Figure 3. In this microstructure, Fe was detected in the matrix except Zn, Sn and S elements. Cu-Sn and Cu-Zn phases were formed between the dendrite arrows of the S2 Sample. In this phase mixture, Cu_3Sn_8 (light gray), and $(Cu, Fe)_3P$ + $CuSn_5$ phase mixture were formed. As seen in Figure 4a–b, the phases formed in S2 and S3 were detected by XRD. In addition, Zn, Sn and S elements were determined in all samples (Figure 2a–d). The difference between the microstructure

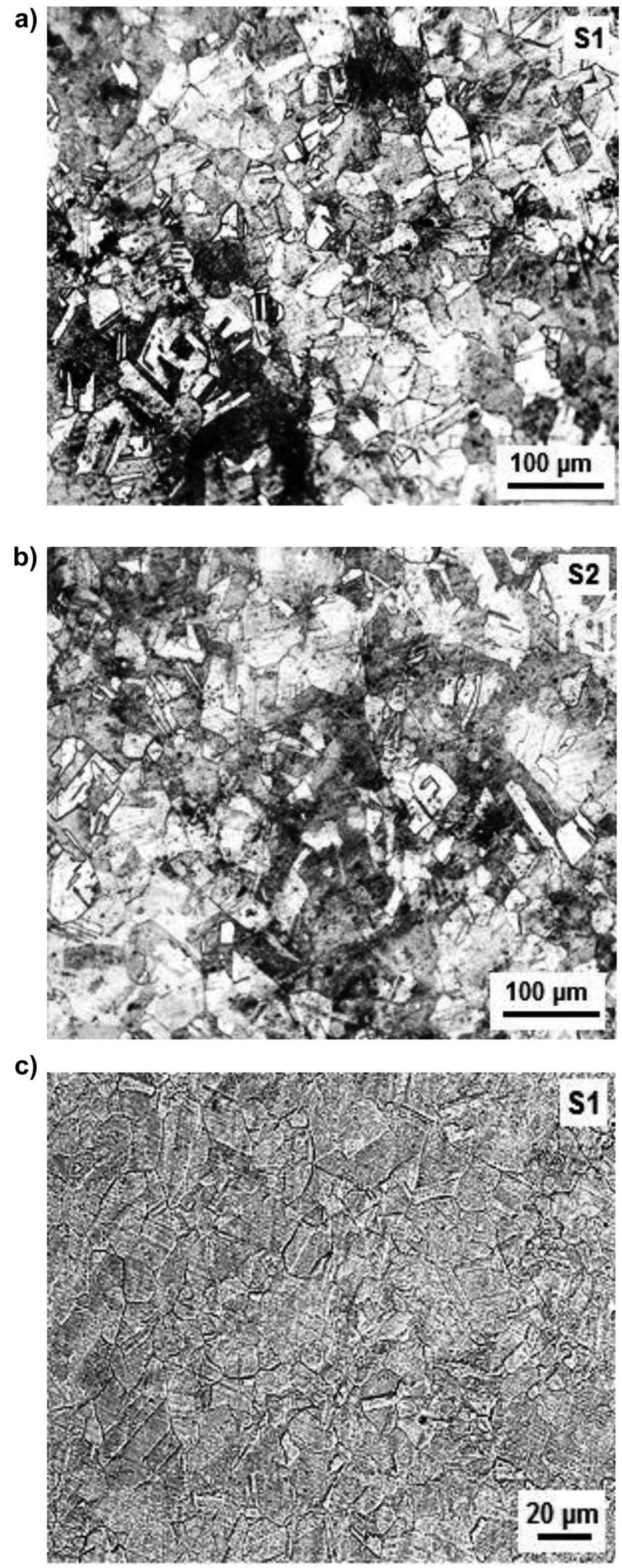

Figure 1: a) Optical image of S1, b) optical image of S2 and c) SEM micrograph of S1.

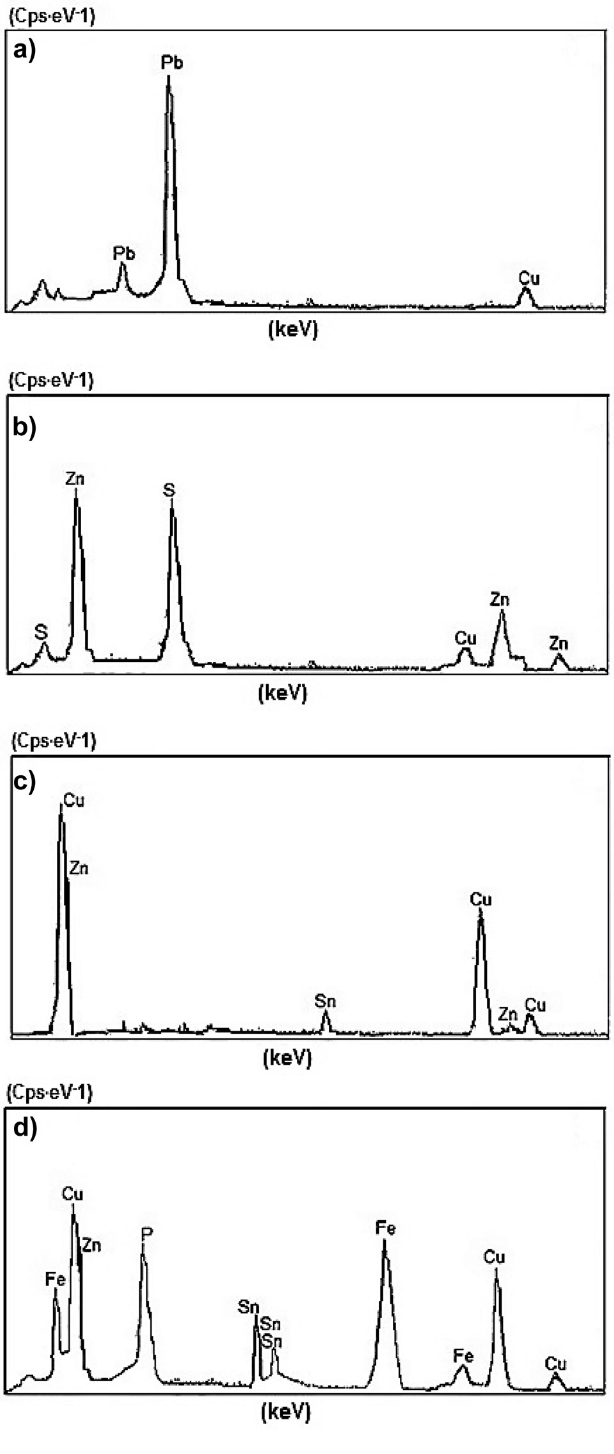

Figure 2: a) EDS analysis of S2 for Pb particles, b) EDS analysis of S2 for (Zn, Cu)S phases, c) EDS analysis of S1 for surface and d) EDS analysis of S3 for interdendritic area.

of S1 and S2 came out due to the formation of ferrous and (Cu, Fe)$_3$ phase. Because, these phases hindered (Zn, Cu)S phase in S3 as seen in Figure 3.

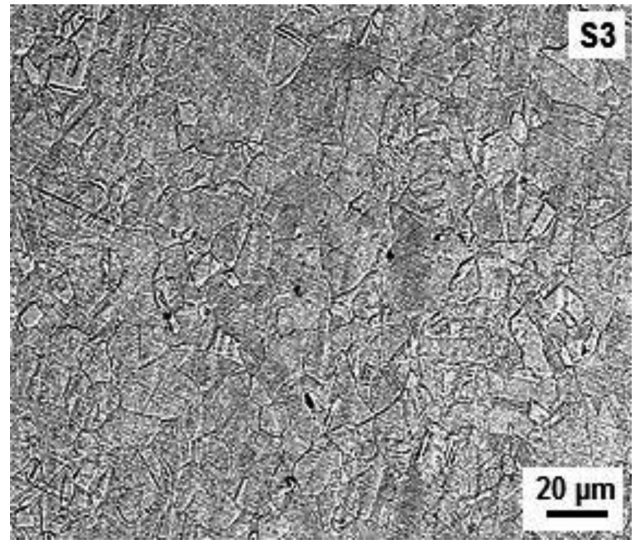

Figure 3: SEM micrograph of S3.

3.2 Effect of Mn

SEM micrograph of S4 is given in Figure 5. As seen in this figure, the matrix of this sample was α-Cu. The phase different from the matrix and placed between the dendrite arrows had more Sn and less Zn than the matrix. Also, the third phase, containing more Sn than the other phases, was an intermetallic compound of Cu-Sn and was located in the middle of the phase between the dendrite arrows [14]. EDS analysis of MnS phase in S4 is illustrated in Figure 6. MnS phases detected at the matrix. The difference between the S1 and S5 samples was that manganese prevented (Zn, Cu)S formation in the S5 Sample and the MnS phase was formed.

3.3 Effect of P

The SEM micrographs of S5, S6 and S7 are given in Figure 7a–c. The microstructures of S5, S6 and S7 were similar to each other. As can be seen from this figure, many different stages were identified. The first phase was the phase between the dendrite arrows and different from the matrix. The second was the phase containing Cu_3P precipitates and (Zn, Cu)S compounds settled in the first phase. However, small $SnPbS_2$ precipitates were seen in spherical form both in the matrix and between the dendrite arrows (Figure 7a–c).

On the other hand, insoluble Zn and Sn elements in the matrix were pushed by the dendrite arrows, causing the formation of Cu-Sn, Cu-Zn and Zn-Sn intermetallic phases.

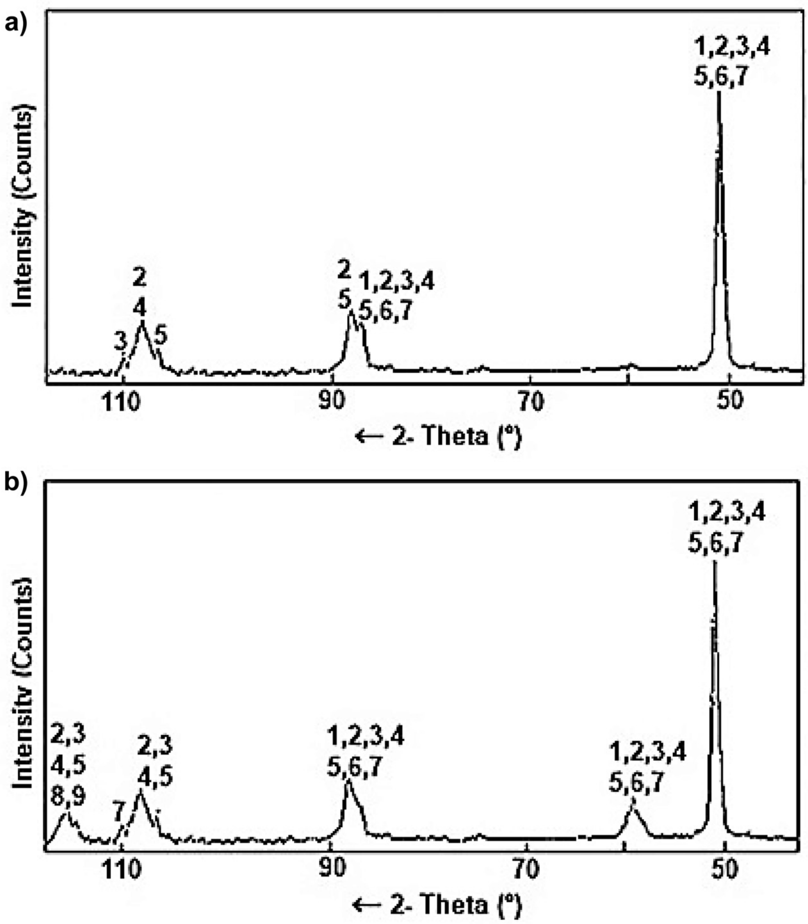

Figure 4: X-ray analysis results of a) S2 (1. α-Cu, 2. $Cu_{31}Sn_8$, 3. Cu_6Sn_5, 4. $ZnSn_2$, 5. $PbSnS_2$, 6. ZnS, 7. Cu_2S), b) S3 (1. α-Cu, 2. $Cu_{31}Sn_8$, 3. Cu_6Sn_5, 4. $ZnSn_2$, 5. $PbSnS_2$, 6. Cu_2S, 7. $FeZn_9$, 8. $FeZn_{21}$ and 9. Cu_5FeS_4).

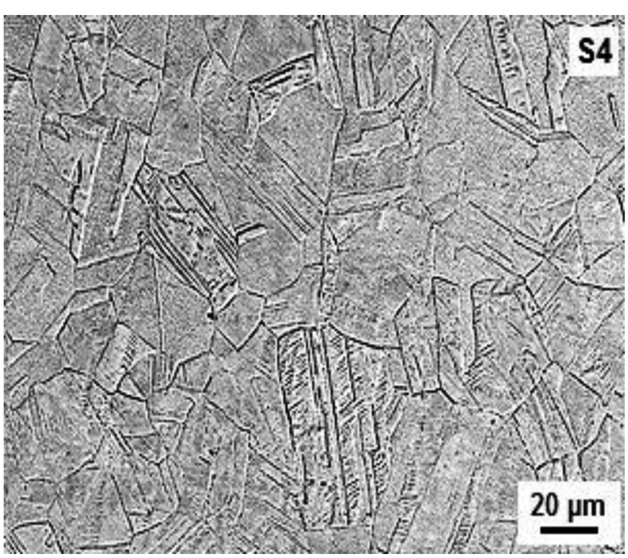

Figure 5: SEM micrograph of S4.

However, Sn that could not be solved in the dendrite arrows diffusing towards the center of the second phase caused the formation of Cu-Sn intermetallic phases, which finally solidified in the second phase [15, 16]. Also (Cu, Zn)S phases solidified around Cu-Sn intermetallic, and the Cu_3P phase solidified around (Cu, Zn)S. EDS analysis of Cu-Zn, Zu-Sn and Zn-Sn intermetallic phases in S5 Sample are given in Figure 8. XRD analysis of these structures is presented in Figure 9.

3.4 Analysis of mechanical behaviour

S-N diagrams of S1–S7 samples are shown in Figure 10. As Fe and Mn formed intermetallic phases, it decreased fatigue resistance. The increase in wt% P increased the fatigue life. The fatigue life of Sn-Cu bronze material was optimally affected by phosphorus. The positive effect of P on tensile

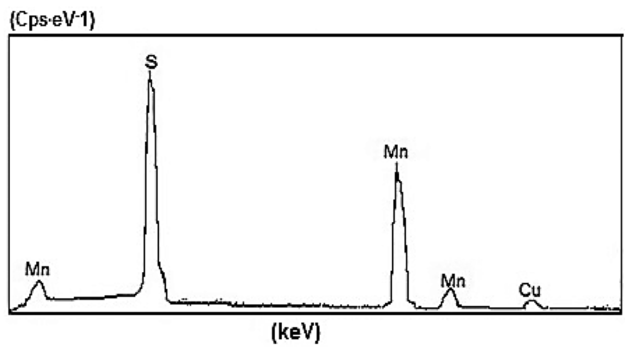

Figure 6: EDS analysis of MnS phase in S4.

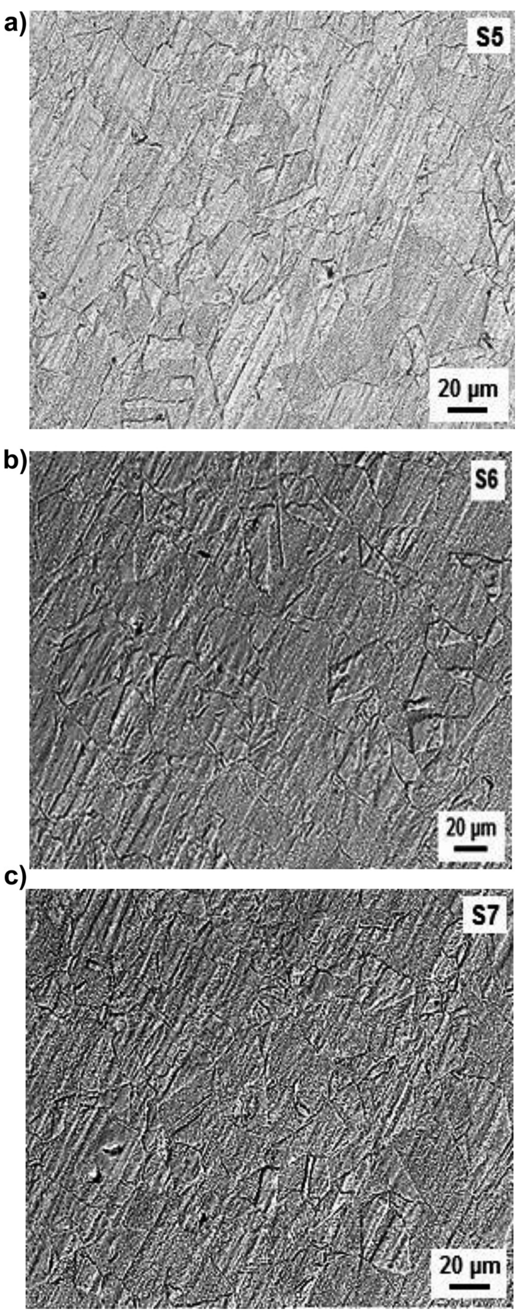

Figure 7: The microstructure view of a) S5, b) S6 and c) S7 by SEM micrograph.

strength and fatigue life increased with the formation of Cu_3P phase around (Zn, Cu)S phases and the formation of Cu-Sn phase in the interdendritic area (Figure 7). The surrounding of Cu_3P around (Zn, Cu)S was compacted and nucleated as small particles around S caused higher tensile strength and higher fatigue life due to their small size [17, 18].

The relation between fatigue strength and surface hardness is given in Figure 11. The relation between fatigue strength and toughness is shown in Figure 12. The relation between fatigue life and tensile strength is demonstrated in Figure 13. As seen from the diagrams in Figures 10, 11, 12, and 13 for S2 and S3, tensile strength and surface hardness increased and %elongation reduced because of the dissolution of Fe in matrix and the precipitation of the phases (Fe-P, Fe-Zn, Fe-Sn and others) in matrix and between dendrite arrows. Tensile strength and fatigue life increased with increasing Fe concentration (Figure 10). In the analysis performed on the fracture surface of the Fe added samples, $PbSnS_2$ and (Zn, Cu)S particles were determined on the fracture surface. Tensile strength and fatigue life values were compared in Figure 13. It was seen that Mn increased fatigue life, hardness and tensile strength. In particular, the increase in fatigue life and tensile strength in the Sample S4 was due to the formation of MnS and the inhibition of the formation of (Zn, Cu)S phases, which were harder and more brittle than MnS [19, 20]. Phosphorus additions increased the yield strength, surface hardness and elongation percentage of S5, S6 and S7 samples. It did not affect tensile strength, but reduced toughness. However, fatigue life significantly increased.

Figure 14 shows SEM micrograph of the fatigue fracture surface of Sample S2. This zone was the center of fatigue crack composed of $PbSnS_2$ particles. The increase in the amount of $PbSnS_2$ particles in the matrix reduced the fatigue life of the samples under high plastic deformation [21–24]. This was a result of crack formation that was propagated between $PbSnS_2$ particles and matrix. In addition, the expansion of these phases and the separation of atoms increased the likelihood of cracking at the interface of these particles and the matrix. Also, decreasing the distance between particles increased crack density. However, Fe inhibited Pb decomposition. So, Sample S2 had a higher fatigue life than Sample S1. The SEM micrograph of the fatigue fracture surface of S4 is indicated in Figure 15. Fatigue lines were detected around the MnS phases and in the matrix. Figure 16 shows SEM micrograph of the fatigue fracture surface of S7 Sample. The matrix and dendritic structures showed different fracture characters, and the part showing the fatigue lines was dendrite arrows.

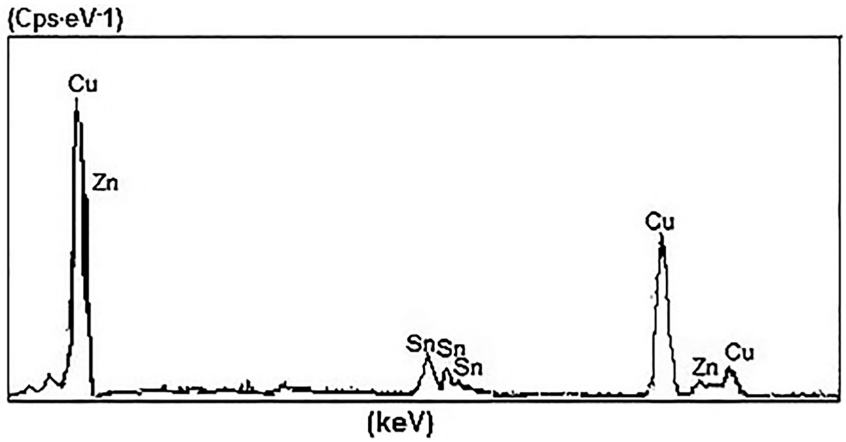

Figure 8: EDS analysis of Cu-Zn, Cu-Sn and Zn-Sn intermetallic phases in S5 sample.

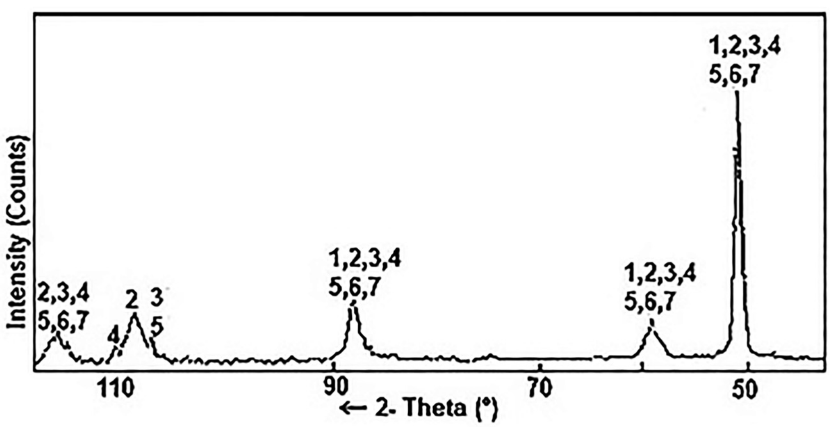

Figure 9: X-ray diffraction of S1 (1. α-Cu, 2. $Cu_{31}Sn_8$, 3. Cu_6Sn_5, 4. $ZnSn_2$, 5. $PbSnS_2$, 6. Cu_2S and 7. Cu_3P).

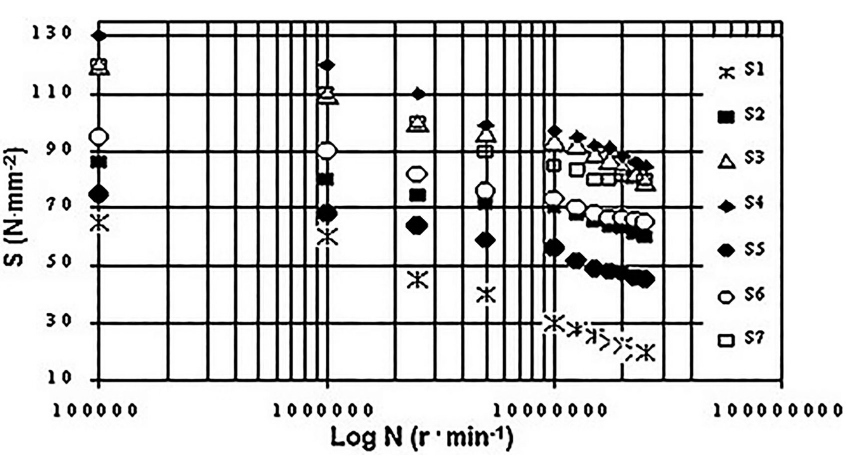

Figure 10: S-N diagrams of S1–S7 samples.

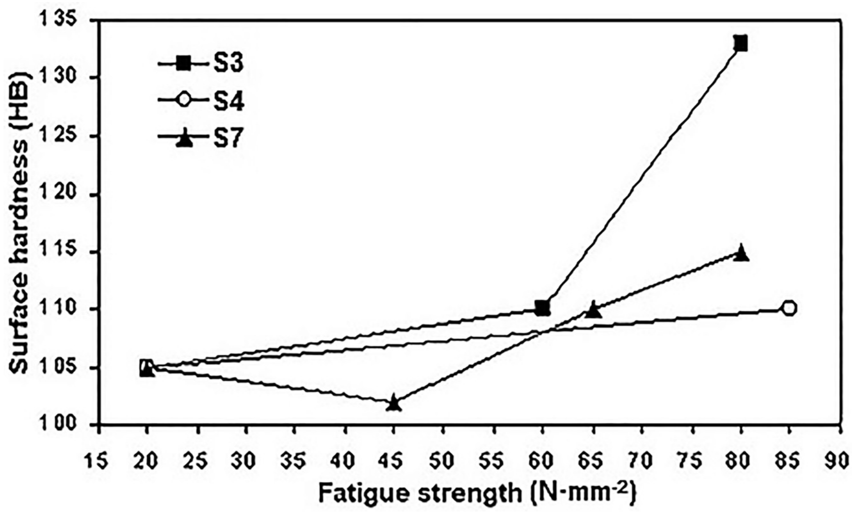

Figure 11: The relation between fatigue strength and surface hardness.

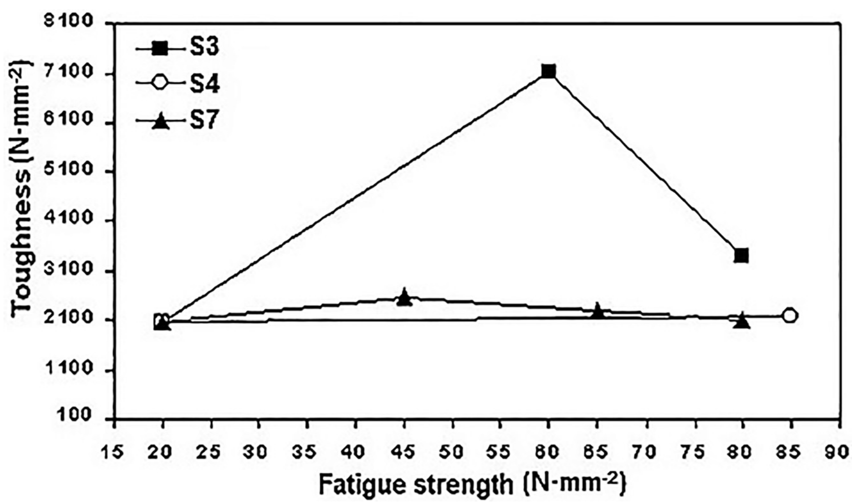

Figure 12: The relation between fatigue strength and toughness.

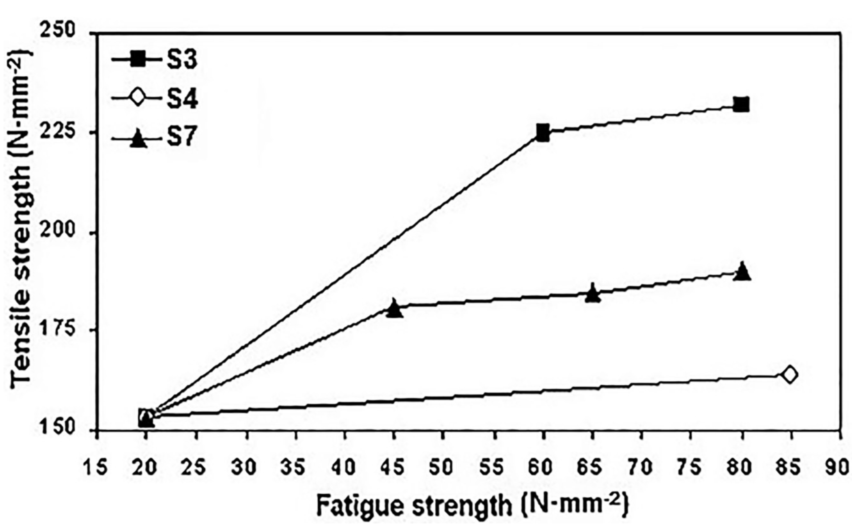

Figure 13: The relation between fatigue life and tensile strength.

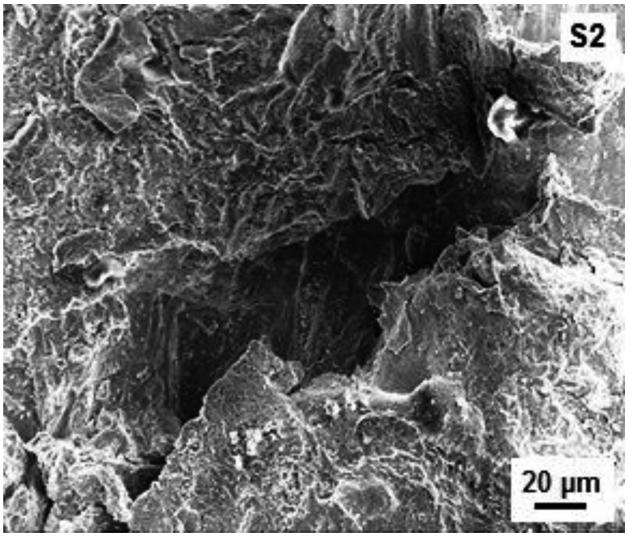

Figure 14: SEM micrograph of the fatigue fracture surface of S2 sample.

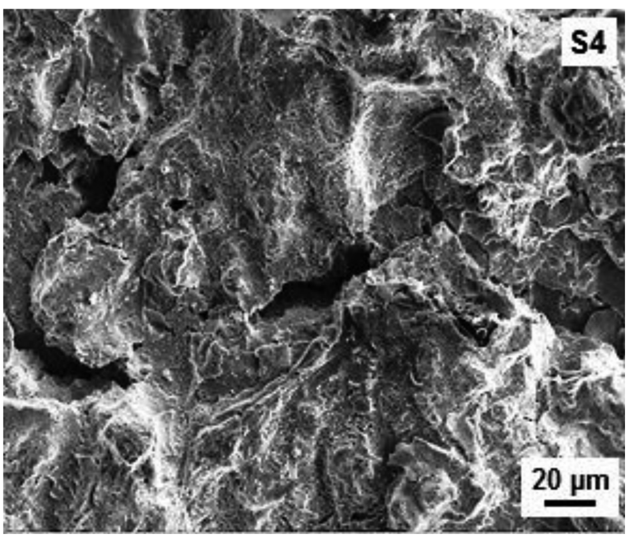

Figure 15: SEM micrograph of the fatigue fracture surface of S4 sample.

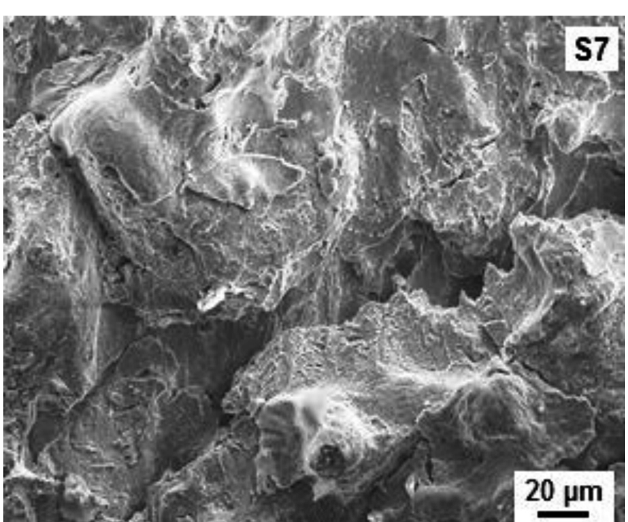

Figure 16: SEM micrograph of the fatigue fracture surface of S7 sample.

4 Conclusions

The addition of Fe first limited the growth of the (Zn, Cu) S phase and then affected the Pb decomposition by allowing the formation of ferrous phases.

The spread of ferrous phases caused an increase in mechanical properties such as surface hardness and tensile strength. On the other hand, it negatively affected elongation.

Mn addition prohibited the formation of (Zn, Cu)S phase, which was a brittle, hard and unwanted phase, and this limitation increased fatigue life.

Fe, Mn and P elements increased fatigue life. The beneficial effect of P addition on the fatigue life far surpassed that of Mn and Fe additives.

Like Mn and Fe, the addition of P affected the (Zn, Cu)S phase and prevented its growth. It increased tensile strength, fatigue life.

Acknowledgement: The authors were grateful to Kayalar Copper Industry and Trade Incorporated Company for their assistance in conducting the experiments.
Author contributions: All the authors have accepted responsibility for the entire content of this submitted manuscript and approved submission.
Research funding: None declared.
Conflict of interest statement: No potential conflict of interest was reported by the authors.

References

[1] W. Chen, M. Wang, Z. Li, et al., “A novel Cu-10Zn-1.5Ni-0.34Si alloy with excellent mechanical property through precipitation hardening,” *J. Mater. Eng. Perform.*, vol. 25, pp. 4624–4630, 2016, https://doi.org/10.1007/s11665-016-2354-3.
[2] S. Zhang, H. Zhu, Z. Hu, X. Zeng, and F. Zhong, “Selective laser melting of Cu-10Zn alloy powder using high laser power,” *Powder Technol.*, vol. 342, pp. 613–620, 2019, https://doi.org/10.1016/j.powtec.2018.10.002.
[3] Q. Liu and L. Cheng, “Structural evolution and electronic properties of Cu-Zn alloy clusters,” *J. Alloys Compd.*, vol. 71, pp. 762–768, 2019, https://doi.org/10.1016/j.jallcom.2018.08.033.
[4] S. Rui, J. Xiaosong, J. Jiaxin, and Z. Degui, “Microstructure and mechanical properties of nano-carbon reinforced Cu-based powder metallurgy friction materials produced by hot isostatic pressing,” *Mater. Test.*, vol. 60, no. 9, pp. 809–817, 2018, https://doi.org/10.3139/120.111217.
[5] A. Choubey, H. Yu, M. Osterman et al., “Intermetallics characterization of lead-free solder joints under isothermal aging,” *J. Electron. Mater.*, vol. 37, pp. 1130–1138, 2008, https://doi.org/10.1007/s11664-008-0466-8.
[6] A. Sharif and Y. Chan, “Dissolution kinetics of BGA Sn–Pb and Sn–Ag solders with Cu substrates during reflow,” *Mater. Sci. Eng. B*, vol. 106, no. 2, pp. 126–131, 2004, https://doi.org/10.1016/j.mseb.2003.09.004.

[7] N. Mookam and K. Kanlayasiri, “Evolution of intermetallic compounds between Sn-0.3 Ag-0.7 Cu low-silver lead-free solder and Cu substrate during thermal aging,” *J. Mater. Sci. Technol.*, vol. 28, no. 1, pp. 53–59, 2012, https://doi.org/10.1016/S1005-0302(12)60023-1.
[8] S. Li and Y. F. Yan, “Intermetallic growth study at Sn-3.0Ag-0.5Cu/Cu solder joint interface during diferent thermal conditions,” *J. Mater. Sci.: Mater. Electron.*, vol. 26, pp. 9470–9477, 2015, https://doi.org/10.1007/s10854-015-3406-4.
[9] B. Liu, T. K. Lee, and K. C. Liu, “Impact of 5% NaCl salt spray pretreatment on the long-term reliability of wafer-level packages with Sn-Pb and Sn-Ag-Cu solder interconnects,” *J. Electron. Mater.*, vol. 40, pp. 2111–2118, 2001, https://doi.org/10.1007/s11664-011-1705-y.
[10] L. M. Satizabal, D. Costa, P. B. Moraes, A. D. Bortolozo, and W. R. Osòrio, “Microstructural array and solute content affecting electrochemical behavior of Sn Ag and Sn Bi alloys compared with a traditional Sn Pb alloy,” *Mater. Chem. Phys.*, vol. 223, pp. 410–425, 2019, https://doi.org/10.1016/j.matchemphys.2018.11.003.
[11] Z. Guo and H. Conrad, “Effect of microstructure size on deformation kinetics and thermo-mechanical fatigue of 63Sn37PB solder joints,” *J. Electron. Packag.*, vol. 118, no. 2, pp. 49–54, 1996, https://doi.org/10.1115/1.2792131.
[12] K. C. Rabell and Y. L. Shen, “Deformation induced phase rearrangement in near eutectic tin–lead alloy,” *Acta Mater.*, vol. 50, no. 12, pp. 3193–3204, 2002, https://doi.org/10.1016/S1359-6454(02)00135-0.
[13] T. Hebesberger, H. P. Stuwe, A. Vorhauer, F. Wetscher, and R. Pippan, “Structure of Cu deformed by high pressure torsion,” *Acta Mater.*, vol. 53, no. 2, pp. 393–402, 2005, https://doi.org/10.1016/j.actamat.2004.09.043.
[14] B. S. Ünlü, A. M. Pınar, and K. Özdin, “Tribological properties of Sn-Pb based SnPbAlZn journal bearings,” *Mater. Test.*, vol. 54, no. 10, pp. 713–717, 2012, https://doi.org/10.3139/120.110375.
[15] D. Song, R. Wang, W. B. Liu, and X. He, “Microstructure and mechanical properties of PbSn alloys deposited on carbon fiber reinforced epoxy composites,” *J. Alloys Compd.*, vol. 505, no. 1, pp. 348–351, 2010, https://doi.org/10.1016/j.jallcom.2010.06.067.
[16] V. V. Popov, E. N. Popova, A. V. Stolbovsky, and R. M. Falahutdinov, “Evolution of the structure of Cu–1% Sn bronze under high pressure torsion and subsequent annealing,” *Phys. Met. Metallogr.*, vol. 119, pp. 358–367, 2018, https://doi.org/10.1134/S0031918X18040154.
[17] Y. Gao, R. O. Ritchie, M. Kumar, and R. K. Nalla, “High-cycle fatigue of nickel-based superalloy ME3 at ambient and elevated temperatures: role of grain-boundary engineering,” *Metall. Mater. Trans. A*, vol. 36, pp. 3325–3333, 2005, https://doi.org/10.1007/s11661-005-0007-5.
[18] J. P. Lucas, H. Rhee, F. Guo, and K. N. Subramanian, “Mechanical properties of intermetallic compounds associated with Pb-free solder joints using nanoindentation,” *J. Electron. Mater.*, vol. 32, pp. 1375–1383, 2003, https://doi.org/10.1007/s11664-003-0104-4.
[19] M. Nagata and M. Fujita, “Evaluation of tribological properties of bearing materials for marine diesel engines utilizing acoustic emission technique,” *Tribol. Int.*, vol. 46, pp. 183–189, 2012, https://doi.org/10.1016/j.triboint.2011.05.026.
[20] P. V. Kuznetsov, T. V. Rakhmatulina, I. V. Belyaeva, and A. V. Korznikov, “Energy of internal interfaces as a characteristic of the structural evolution of ultrafine-grained copper and nickel after annealing,” *Phys. Met. Metallogr.*, vol. 118, pp. 241–248, 2017, https://doi.org/10.1134/S0031918X17030115.
[21] A. Das, “Grain boundary engineering: fatigue fracture,” *Philos. Mag.*, vol. 97, no. 11, pp. 850–867, 2017, https://doi.org/10.1080/14786435.2017.1285072.
[22] D. K. Orlova, T. I. Chashchukhina, L. M. Voronova, and M. V. Degtyarev, “Effect of temperature–strain rate conditions of deformation on structure formation in commercially pure copper deformed in Bridgman anvil,” *Phys. Met. Metallogr.*, vol. 116, pp. 951–958, 2015, https://doi.org/10.1134/S0031918X15090136.
[23] T. I. Chashchukhina, M. V. Degtyarev, and L. M. Voronova, “Effect of pressure on the evolution of copper microstructure upon large plastic deformation,” *Phys. Met. Metallogr.*, vol. 109, pp. 201–209, 2010, https://doi.org/10.1134/S0031918X10020122.
[24] O. Fumio, H. Noritake, and I. Takamoto, “Evaluation of the low-cycle fatigue strength of Sn3.0Ag0.5Cu solder at 313 and 353 K using a small specimen,” *Mater. Test.*, vol. 61, no. 8, pp. 719–723, 2019, https://doi.org/10.3139/120.111376.

The authors of this contribution

Tanju Teker
Prof. Dr. Tanju Teker, born in Sivas in 1971, works in Sivas Cumhuriyet University, Faculty of Technology, Department of Manufacturing Engineering, Sivas, Turkey. He graduated in Metallurgy Education from Gazi University, Ankara, Turkey, in 1997. He received his MSc and PhD degrees from Firat University, Elazig, Turkey, in 2004 and 2010, respectively. His research interests metal coating techniques, casting, fusion and welding solid-state welding methods.

S. Osman Yılmaz
Prof. Dr. S. Osman Yılmaz, born in Elazig in 1966, works in Namık Kemal University, Faculty of Engineering, Department of Mechanical Engineering, Corlu, Tekirdağ, Turkey. He received his BSc from METU University, Ankara, Faculty of Engineering, Metallurgy and Materials Engineering Department in 1989, his MSc from the Institute of Science and Technology, Metallurgy Department in 1992 and his Ph.D from the University of Firat, Institute of Science and Technology, Metallurgy Department, Elazig, in 1998. He studied metal coating techniques, surface modification, welding, casting and wear.

Ercan Bulus
Assoc. Prof. Dr. Ercan Bulus, born in Kırklareli in 1966, works in Namık Kemal University, Faculty of Engineering, Department of Computer Engineering, Corlu, Tekirdağ, Turkey. He received his BSc from University of Trakya, Edirne, Faculty of Science and Literature, Physics Department in 1988, his MSc from the Trakya University, the Institute of Science and Technology, Physics Department in 1992 and his Ph. D from the Trakya University, Institute of Science and Technology, Department of Computer Engineering, Edirne, in 1995. He studied cryptology, computer and network security, deep learning programming.